Inorganic Chemistry

Article

pubs.acs.org/IC

Oxo-Bridge Scenario behind Single-Site Water-Oxidation Catalysts

Isidoro López,[†] Somnath Maji,[†] J. Benet-Buchholz,[†] and Antoni Llobet*[,†,‡]

[†]Institute of Chemical Research of Catalonia (ICIQ), Av. Països Catalans, 16, 43007 Tarragona, Spain

[‡]Departament de Química, Universitat Autònoma de Barcelona, Cerdanyola del Vallès, 08193 Barcelona, Spain

Supporting Information

ABSTRACT: High-oxidation-state decay of mononuclear complexes $[RuTB(H_2O)]^{2+}$ ($\mathbf{X}^{2+}$, where B = 2,2′-bpy or bpy for X = 1; B = 5,5′-F_2-bpy for X = 2; B = 6,6′-F_2-bpy for X = 3; T = 2,2′:6′,2″-terpyridine) oxidized with a large excess of Ce^{IV} generates a manifold of polynuclear oxo-bridged complexes. These include the following complexes: (a) dinuclear [TB-Ru^{IV}-O-Ru^{IV}-(T)(O)OH_2]$^{2+}$ (**1-dn**$^{4+}$), [TB-Ru^{III}-O-Ru^{III}-T-$(MeCN)_2$]$^{4+}$ (**1-dn-N**$^{4+}$), and {[Ru^{III}(trpy)(bpy)]$_2$(μ-O)}$^{4+}$ (**1-dm**$^{4+}$); (b) trinuclear {[Ru^{III}(trpy)(bpy)(μ-O)]$_2$$Ru^{IV}$(trpy)-$(H_2O)$}$(ClO_4)_5$$^{6+}$ (**1-tr**$^{6+}$) and {[Ru^{III}(trpy)(bpy)(μ-O)]$_2$$Ru^{IV}(pic)_2$}$(ClO_4)_4$ (**1-tr-P**$^{4+}$, where P is the 2-pyridinecarboxylate anion); and (c) tetranuclear [TB-Ru^{III}-O-TRu^{IV}(H_2O)-O-TRu^{IV}(H_2O)-O-Ru^{III}-TB]$^{8+}$ (**1-tn**$^{8+}$), [TB-Ru^{III}-O-TRu^{IV}(AcO)-O-TRu^{IV}(AcO)-O-Ru^{III}-TB]$^{6+}$ (**1-tn-Ac**$^{6+}$), and [TB-Ru^{II}-O-TRu^{IV}(MeCN)-O-TRu^{IV}(MeCN)-O-Ru^{II}-TB]$^{6+}$ (**1-tn-N**$^{6+}$). These complexes have been characterized structurally by single-crystal X-ray diffraction analysis, and their structural properties were correlated with their electronic structures. Dinuclear complex **1-dm**$^{4+}$ has been further characterized by spectroscopic and electrochemical techniques. Addition of excess Ce^{IV} to **1-dm**$^{4+}$ generates dioxygen in a catalytic manner. However, resonance Raman spectroscopy points to the in situ formation of **1-dn**$^{4+}$ as the active species.

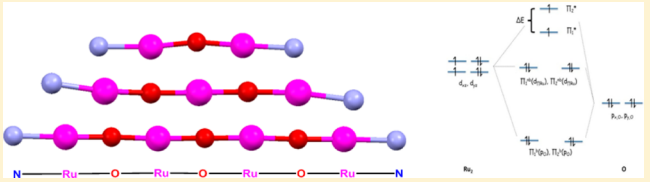

1. INTRODUCTION

The oxo-bridged metal unit is a ubiquitous motif in bioinorganic chemistry. There are a large number of metalloproteins[1−3] that contain the Fe-O-Fe core, whereas the oxygen-evolving complex (OEC) of photosystem II (PSII) contains Mn-O-Mn units within its $CaMn_4$ cluster. The latter has gained increasing attention because it performs the key reaction that needs to be fully understood and mastered for the development of commercial devices for the efficient conversion of sunlight into chemical fuels such as H_2 or CH_3OH.

To mimic the functional properties of an OEC, many polynuclear μ-oxo metal complexes with high oxidation states have been synthesized. The blue dimer was the first-reported molecularly well-characterized water oxidation catalyst (WOC), and it contains a Ru^{III}-O-Ru^{III} unit. Other recently reported polynuclear WOCs include complexes with rigid aromatic organic-bridging ligands instead of the oxo bridge[4−8] as well as a family of polyoxometalate complexes.[9−12]

However, the recent discovery of single-site WOCs[5,13,14] has generated a large body of complexes that are proposed to remain mononuclear species during the catalytic cycle. The successive pathways that lead to the evolution of dioxygen in complexes related to $[RuTB(H_2O)]^{2+}$ ($\mathbf{X}^{2+}$, where B = 2,2′-bpy or bpy for X = 1; B = 5,5′-F_2-bpy for X = 2; B = 6,6′-F_2-bpy for X = 3; and T = 2,2′:6′,2″-terpyridine) have been extensively studied,[13,15] and the accepted mechanism considers the key O−O-bond-forming step to be a water nucleophilic attack on a Ru^{V}-O moiety. Although this description is now widely accepted,[16,17] the corresponding deactivation pathways associated with this type of catalyst have not been reported. In this regard, only the potential dissociation of bpy and its subsequent oxidation to 2,2′-bipyridine *N*,*N*-dioxide has been pointed[18] out as a hypothetical decomposition path.

Recently, our group has found[19] that mononuclear complexes partially transform to dinuclear oxo-bridge structures of the general formula [TB-Ru^{IV}(μ-O)Ru^{IV}T(O)(H_2O)]$^{4+}$ (**X-dn**$^{4+}$; X = 1, 2 or 3) when high oxidation states are reached. The generation of these dinuclear complexes necessarily involves the release of bpy from the first coordination sphere of the initial complex. The dinuclear complexes thus formed are active and rugged WOCs, and their presence complements the accepted mechanism, showing that the system is much more complex than originally described. Furthermore, the formation of these μ-oxo structures uncovers a tendency for the production of oxo-bridge oligomers by mononuclear Ru complexes in high oxidation states, as happens with Fe[2,20] and Cu.[20−22]

In the present Article, we examine the interconnection between μ-oxo species generated after the chemical and electrochemical oxidation of mononuclear complexes related to [TB-Ru^{II}(H_2O)]$^{2+}$ (**1**$^{2+}$) and discuss structural and electronic parameters.

2. EXPERIMENTAL METHODS

2.1. Materials. All reagents used in the present work were obtained from Aldrich Chemical and were used without further purification. $RuCl_3 \cdot 3H_2O$ was supplied by Alfa Aesar and was used as received. Trifluoromethanesulfonic acid (HOTf) was obtained from CYMIT. Reagent-grade organic solvents were obtained from SDS, and high-

Received: October 28, 2014
Published: December 29, 2014

DOI: 10.1021/ic502603e
Inorg. Chem. 2015, 54, 658−666

purity deionized water was obtained by passing distilled water through a nanopure Milli-Q water purification system.

2.2. Preparations. $[Ru(trpy)(bpy)(H_2O)](PF_6)_2$ ($\mathbf{1}^{2+}$),[23] $[Ru(trpy)(5,5'\text{-}F_2\text{-}bpy)(H_2O)](PF_6)_2$ ($\mathbf{2}^{2+}$),[24] $[Ru(trpy)(6,6'\text{-}F_2\text{-}bpy)(H_2O)](PF_6)_2$ ($\mathbf{3}^{2+}$),[24] $[(trpy)(bpy)Ru^{IV}(\mu\text{-}O)Ru^{IV}(trpy)(O)(H_2O)](ClO_4)_4$ (**1-dn**$^{4+}$),[19] and $[(trpy)(5,5'\text{-}F_2\text{-}bpy)Ru^{IV}(\mu\text{-}O)Ru^{IV}(trpy)(O)(H_2O)](ClO_4)_4$ (**2-dn**$^{4+}$)[19] were prepared as described in the literature.

*2.2.1. {[Ru(trpy)(bpy)]$_2$(μ-O)}(ClO$_4$)$_4$·7H$_2$O (**1-dm**$^{4+}$).* $[Ru(trpy)(bpy)(H_2O)](PF_6)_2$ (101.4 mg, 0.127 mmol) was dissolved in 0.1 M HOTf (127 mL), and then 100 equiv of $(NH_4)_2Ce(NO_3)_6$ (7.10 g, 12.7 mmol, dissolved in the minimum amount of 0.1 M HOTf) was added. The solution was left stirred for approximately 1 week and UV−vis monitored periodically. When the band at 688 nm seemed to achieve a maximum value, a saturated aqueous solution of $NaClO_4$ (7 mL) was added. A dark-green solid precipitated and was filtered and washed with some drops of cold water. The solid was collected and dried under vacuum overnight. Yield: 39.9 mg (45%). Anal. Calcd for $C_{50}H_{50}Cl_4N_{10}O_{23}Ru_2$: C, 39.48; H, 3.45; N, 9.21. Found: C, 39.24; H, 3.24; N, 9.07.

2.3. Preparation of Single Crystals. *2.3.1. [(trpy)(6,6′-F$_2$-bpy)Ru^{IV}(μ-O)Ru^{IV}(trpy)(O)(H$_2$O)](ClO$_4$)$_4$·3H$_2$O (**3-dn**$^{4+}$).* Single crystals of **3-dn**$^{4+}$ could be grown at room temperature 1 week after the addition of some drops of a saturated aqueous $NaClO_4$ solution to a catalytic solution of $\mathbf{3}^{2+}$ in 0.1 M HOTf when oxygen evolution had finished.

*2.3.2. [(trpy)(bpy)Ru^{III}(μ-O)Ru^{III}(trpy)(CH$_3$CN)$_2$](PF$_6$)$_4$·H$_2$O·CH$_3$CN (**1-dn-N**$^{4+}$) and [(trpy)(6,6′-F$_2$-bpy)Ru^{III}(μ-O)Ru^{III}(trpy)(CH$_3$CN)$_2$](PF$_6$)$_4$·CH$_3$CN (**3-dn-N**$^{4+}$).* The starting complex (**1-dn**$^{4+}$ or **3-dn**$^{4+}$, respectively) was dissolved in CH_3CN, and approximately 10 μL of a saturated aqueous solution of NH_4PF_6 was added. Crystals were grown by slow vapor diffusion of Et_2O into the solutions.

*2.3.3. {[Ru^{III}(trpy)(bpy)]$_2$(μ-O)}(ClO$_4$)$_4$·4H$_2$O (**1-dm**$^{4+}$).* Single crystals could be obtained at room temperature 2 days after the addition of some drops of a saturated aqueous $NaClO_4$ solution to a concentrated solution of **1-dm**$^{4+}$ in 0.1 M HOTf.

*2.3.4. {[Ru^{III,5}(trpy)(bpy)]$_2$(μ-O)}(ClO$_4$)$_4$·3/2H$_2$O (**1-dm**$^{5+}$).* Single crystals of **1-dm**$^{5+}$ could be grown at room temperature 5 days after the addition of some drops of a saturated aqueous $NaClO_4$ solution to a catalytic solution of **1-dm**$^{4+}$ in 0.1 M HOTf when oxygen evolution had finished.

*2.3.5. {[Ru^{III}(trpy)(bpy)(μ-O)]$_2$Ru^{IV}(trpy)(H$_2$O)}(ClO$_4$)$_5$(PF$_6$)·2H$_2$O (**1-tr**$^{6+}$).* Single crystals of this complex were grown at room temperature 3 days after the addition of acetone to a solution of **1-dn**$^{4+}$ in 0.1 M HOTf that contained some drops of a saturated aqueous solution of NH_4PF_6. The acetone/water ratio was approximately 1:1.

*2.3.6. {[Ru^{III}(trpy)(bpy)(μ-O)]$_2$Ru^{IV}(pic)$_2$}(ClO$_4$)$_4$ (**1-tr-P**$^{4+}$).* An amount of picolinic acid (10 equiv) was added to a catalytic solution of $\mathbf{1}^{2+}$ in 0.1 M HOTf when oxygen evolution had finished. The formation of **1-tr-P**$^{4+}$ was tracked by monitoring the increase of a band at 688 nm in the UV−vis spectrum. Single crystals were precipitated at room temperature 5 days after the addition of some drops of a saturated aqueous $NaClO_4$ solution to the above solution when the increase of the band was negligible.

*2.3.7. {[(trpy)(5,5′-F$_2$-bpy)Ru^{III}(μ-O)Ru^{IV}(trpy)(CH$_3$COO)]$_2$(μ-O)}(ClO$_4$)$_6$·2H$_2$O (**2-tn-Ac**$^{6+}$), {[(trpy)(bpy)Ru^{II}(μ-O)Ru^{IV}(trpy)(CH$_3$CN)]$_2$(μ-O)}(PF$_6$)$_6$·xCH$_3$CN (**1-tn-N**$^{6+}$), and {[(trpy)(6,6′-F$_2$bpy)Ru^{II}(μ-O)Ru^{IV}(trpy)(CH$_3$CN)]$_2$(μ-O)}(PF$_6$)$_4$(ClO$_4$)$_2$·3/2CH$_3$CN (**3-tn-N**$^{6+}$).* Single crystals for all of these complexes could be obtained by the same procedure. The corresponding dinuclear compounds (**1-dn**$^{4+}$, **2-dn**$^{4+}$, or **3-dn**$^{4+}$) were dissolved in CH_3CN, and approximately 10 μL of a saturated aqueous solution of NH_4PF_6 was added. Crystals were grown by slow vapor diffusion of Et_2O into the solutions.

2.4. Equipment and Measurements. UV−vis spectroscopy was carried out on a Cary 50 (Varian) UV−vis spectrophotometer in 1 cm (or 0.2 cm when indicated) quartz cuvettes. Cyclic voltammetry (CV) and differential pulse voltammetry (DPV) experiments were carried out on an IJ-Cambria CHI-660 or a Bio-Logic SP-150 potentiostat using a three-electrode cell, respectively. Typical CV experiments were carried out at a scan rate of 100 mV s^{-1}. DPV experiments were carried out with the following parameters: pulse height = 50 mV, pulse width = 50 ms, step height = 4 mV, and step time = 200 ms. A glassy-carbon electrode (diameter = 3 mm) was used as the working electrode, platinum wire was used as the auxiliary electrode, and SSCE was used as the reference electrode. The working electrode was polished with 0.05 μm of aluminum paste and rinsed with distilled water and acetone, followed by blow-drying before each measurement. All CV data presented in this Article were recorded in the absence of light and inside of a Faradaic cage. The electrochemical experiments were carried out in 0.1 M CF_3SO_3H (pH 1.0). The $E_{1/2}$ values reported in this Article were estimated from CV experiments as the average of the oxidative and reductive peak potentials ($(E_{p,a} + E_{p,c})/2$) or taken as $E(I_{max})$ from DPV measurements.

NMR spectroscopy was carried out at room temperature on a 400 MHz Bruker Avance II spectrometer or a Bruker Avance 500 MHz spectrometer. Samples were run in 0.1 M DOTf or CD_3CN with internal references (residual protons). Elemental analysis was carried out using an EA-1108 CHNS-O elemental analyzer from Fisons Instruments.

Samples for resonance Raman (RR) spectroscopy were typically prepared by mixing a 1 mM solution of the starting complex with the desired amount of $(NH_4)_2Ce(NO_3)_6$ and then transferring 100 μL of the reaction solution to an aluminum crucible, which was subsequently frozen for an appropriate time in liquid N_2. The crucible was then placed into a Linkam THMS 600 temperature-controlled cryo stage to keep the temperature at −12 °C. The RR spectrum was acquired using a Renishaw inVia Reflex RAMAN confocal microscope (Gloucestershire, U.K.) that was equipped with an Ar-ion laser at 514 nm and a Peltier-cooled CCD detector (−70 °C) coupled to a Leica DM-2500 microscope. Calibration was carried out daily by recording the RR spectrum of an internal Si standard. Rayleigh scattered light was appropriately rejected by using edge-type filters. Spectra were recorded as the accumulation of 5 scans with a 20 s scan time for each. A 10× working-distance microscope objective was used to focus 50% of the laser power (25 mW) onto the sample.

Online manometric O_2 measurements were carried out on a Testo 521 differential pressure manometer with an operating range of 1−100 hPa and an accuracy within 0.5% of the measurement. The manometer was coupled to thermostated reaction vessels for dynamic monitoring of the headspace pressure above each reaction. The manometer's secondary ports were connected to thermostated reaction vessels containing the same solvents and headspace volumes as the sample vials. A typical experiment consisted of the addition of 100 equiv of $(NH_4)_2Ce(NO_3)_6$ (previously dissolved in 100 μL of 0.1 M HOTf) to a solution of the catalyst in 1.850 mL of the same solvent containing the necessary amount of complex to yield a final concentration of 1 mM. This combination is referred to as the catalytic solution herein.

2.5. Single-Crystal X-ray Structure Determination. All measured crystals were prepared under inert conditions and immersed in perfluoropolyether as the protecting oil for manipulation.

2.5.1. Data Collection. Crystal structure determination was carried out using an APEX DUO Kappa 4-axis goniometer equipped with an APEX2 4K CCD area detector, a Microfocus Source E025 IuS using Mo Kα radiation, Quazar MX multilayer optics as the monochromator, and an Oxford Cryosystems low-temperature device (Cryostream 700 Plus, T = −173 °C). Full-sphere data collection was used with ω and φ scans. For data collection and data reduction, we used the software programs APEX2[25] and SAINT, V/.60A,[26] respectively.

2.5.2. Structure Solution and Refinement. Crystal structure solutions were obtained using direct methods as implemented in SHELXTL[27] and visualized using the program XP. Missing atoms were subsequently located from difference Fourier synthesis and added to the atom list. Least-squares refinement on F^2 using all measured intensities was carried out using the program SHELXTL. All nonhydrogen atoms were refined, including anisotropic displacement parameters. In the case of **1-tn-N**$^{6+}$, the program SQUEEZE[28] was applied in order to avoid the highly disordered solvent molecules leading to a refined model with an $R_{(1)}$ value of 6.34% in which all of the solvent molecules were removed. The crystals obtained for **1-tn-N**$^{6+}$ were diffracting extremely weakly so that a completeness of only 93.6% could be reached at a resolution of sin (θ/λ) = 0.6. Compound

DOI: 10.1021/ic502603e
Inorg. Chem. 2015, 54, 658−666

Scheme 1. Synthesis Strategy and Complex Nomenclature[a]

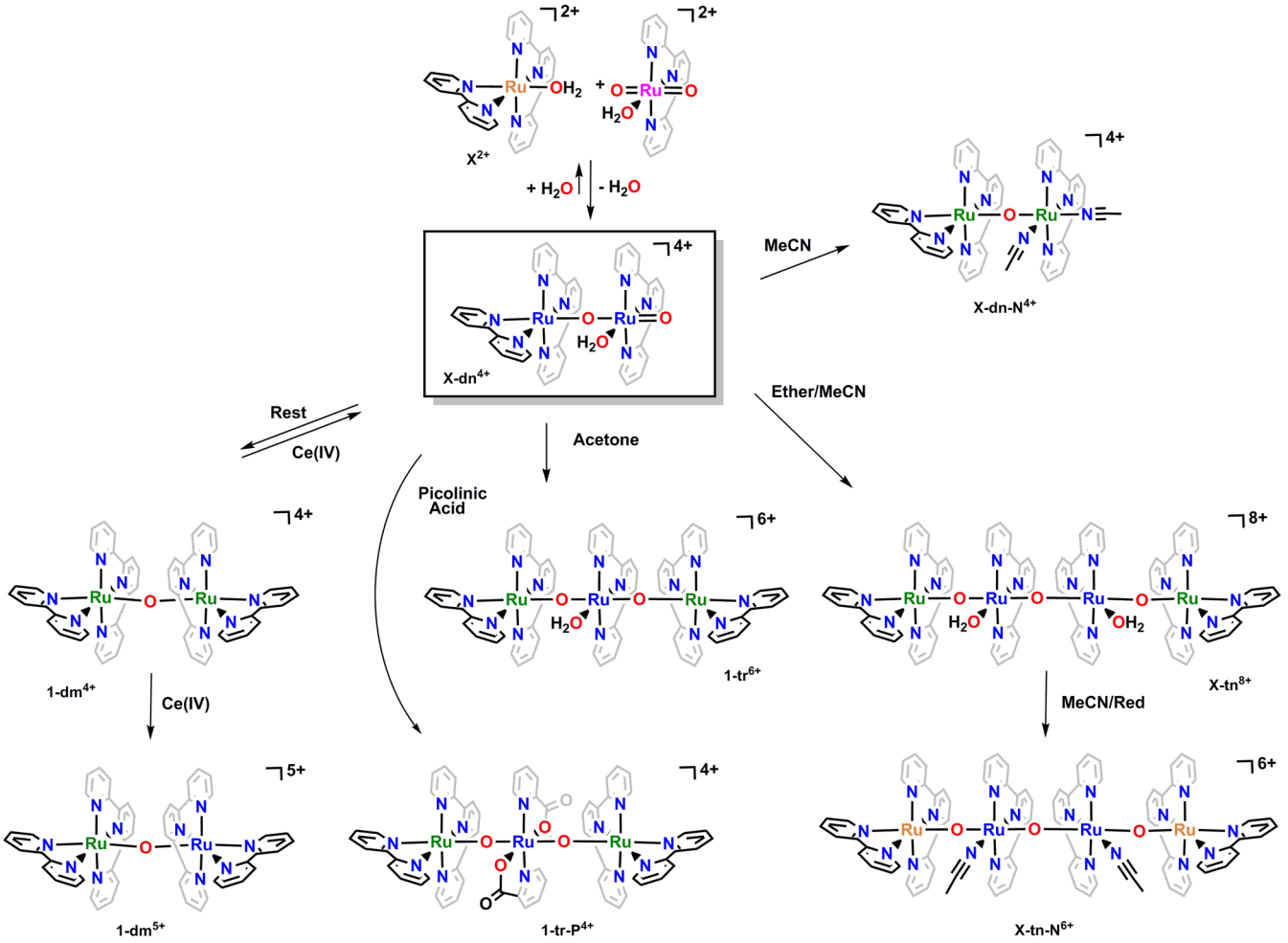

[a]For unsubstituted bpy, X = 1; for 5,5′-F_2-bpy, X = 2; and for 6,6′-F_2-bpy, X = 3. Color codes for formal Ru oxidation states are as follows: fuchsia, VI; blue, IV; green, III; and orange, II.

1-dm^{4+} crystallized as a two-domain crystal (ratio = 73:27). The collected data were processed with TWINABS, taking into account overlapping reflections.

3. RESULTS AND DISCUSSION

3.1. Synthesis. In a previous report,[19] we demonstrated that addition of an excess of Ce^{IV} to WOC $[TB\text{-}Ru^{II}(H_2O)]^{2+}$ ($\mathbf{1}^{2+}$) generates oxygen and that during turnover the bpy ligand slowly falls off of the first coordination sphere and generates $[T\text{-}Ru^{VI}(O)_2(H_2O)]^{2+}$. The latter reacts in turn with $\mathbf{1}^{2+}$ to form dinuclear complex **1-dn**$^{4+}$, as indicated in eq 1 and Scheme 1.

$$[TB\text{-}Ru^{II}\text{-}OH_2]^{2+}(\mathbf{1}^{2+}) + [T\text{-}Ru^{VI}\text{-}(O)_2OH_2]^{2+} \rightleftharpoons [TB\text{-}Ru^{IV}\text{-}O\text{-}Ru^{IV}\text{-}(T)(O)OH_2]^{2+}(\mathbf{1\text{-}dn}^{4+}) + H_2O \quad (1)$$

We have also found qualitative evidence that dinuclear complex **1-dn**$^{4+}$ could be obtained electrochemically from a solution of $\mathbf{1}^{2+}$ after an overnight application of a potential of 1.2 V. This indicates the existence of multiple routes to prepare dinuclear complexes from their respective mononuclear complex and is in agreement with Ce^{IV} acting only as an outer-sphere electron-transfer agent.

One-electron oxidation of **1-dn**$^{4+}$ produces a dinuclear complex in the oxidation state IV,V that is associated with a large electrocatalytic wave responsible for water oxidation. However, **1-dn**$^{4+}$ is also a very strong oxidative reagent, especially toward organic substrates. For instance, addition of MeCN produces the immediate reduction of the dimer to the lower oxidation states III,III, followed by solvent coordination. The latter is indicated in eq 2, maintaining the original Ru-O-Ru backbone.

$$[TB\text{-}Ru^{III}\text{-}O\text{-}Ru^{III}\text{-}T(OH_2)_2]^{4+} + 2MeCN \rightarrow [TB\text{-}Ru^{III}\text{-}O\text{-}Ru^{III}\text{-}T(MeCN)_2]^{4+}(\mathbf{1\text{-}dn\text{-}N}^{4+}) + 2H_2O \quad (2)$$

In an analogous manner, addition of ether/MeCN produces tetranuclear complexes in different oxidation states. As in the previous case, the addition of organic compounds gives rise to the immediate reduction of the initial dinuclear complex, **X-dn**$^{4+}$, followed by an oligomerization process generating,

DOI: 10.1021/ic502603e
Inorg. Chem. 2015, 54, 658−666

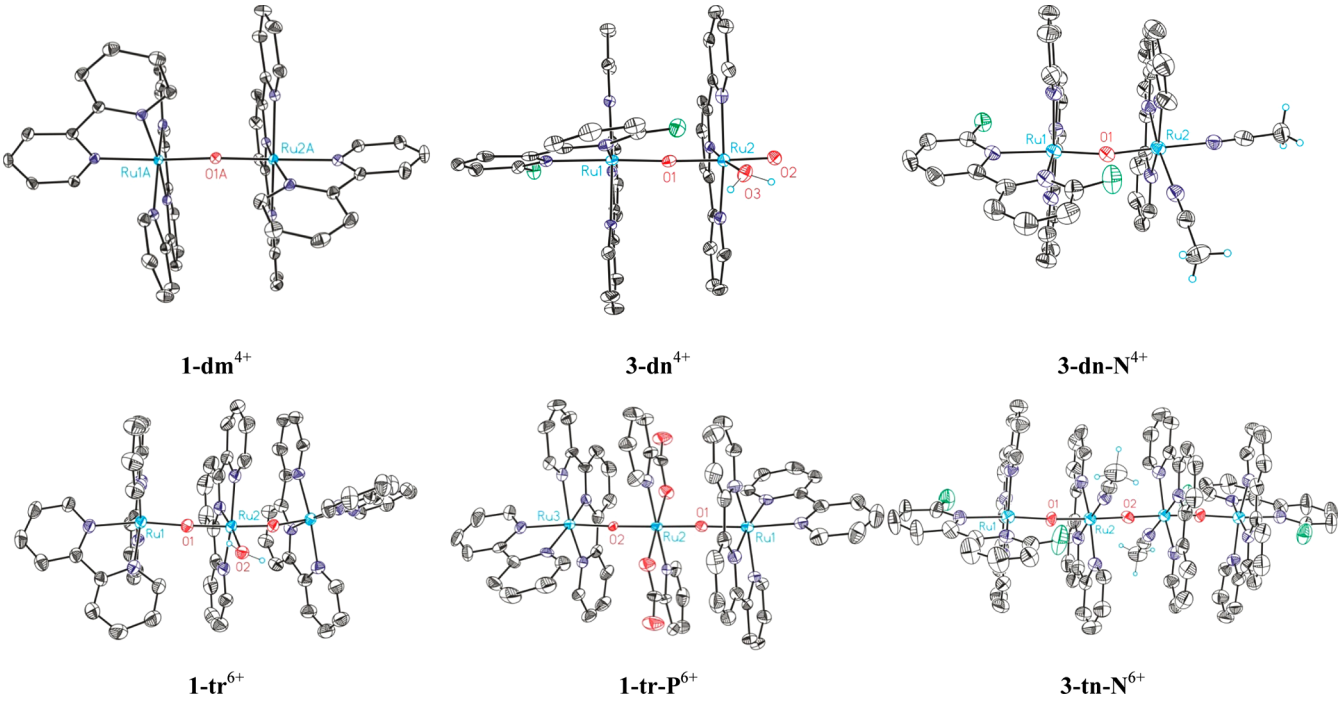

1-dm^{4+} **3-dn**$^{4+}$ **3-dn-N**$^{4+}$

1-tr^{6+} **1-tr-P**$^{6+}$ **3-tn-N**$^{6+}$

Figure 1. ORTEP plots (ellipsoid drawn at 50% probability) of the X-ray structures: cyan, Ru; red, O; blue, N; black, C; and green, F. H atoms are not shown except for the monodentate ligands.

$$[\text{TB-Ru}^{\text{III}}\text{-O-TRu}^{\text{IV}}(\text{H}_2\text{O})\text{-O-TRu}^{\text{IV}}(\text{H}_2\text{O})\text{-O-Ru}^{\text{III}}\text{-TB}]^{8+} (\mathbf{1\text{-}tn}^{8+}) + 2\text{AcO}^- \rightarrow [\text{TB-Ru}^{\text{III}}\text{-O-TRu}^{\text{IV}}(\text{AcO})\text{-O-TRu}^{\text{IV}}(\text{AcO})\text{-O-Ru}^{\text{III}}\text{-TB}]^{6+} (\mathbf{1\text{-}tn\text{-}Ac}^{6+}) + 2\text{H}_2\text{O} \quad (3)$$

where the acetate ligand coordinates in a monodentate terminal fashion. The origin of the acetato ligand is not clear, but it might come from the hydrolysis of MeCN that is catalyzed by Ru complexes, as we and others have shown previously.[29,30]

Further reduction of **1-tn**$^{8+}$ and solvent coordination yields the tetranuclear complexes, **X-tn-N**$^{6+}$, as indicated below.

$$[\text{TB-Ru}^{\text{III}}\text{-O-TRu}^{\text{IV}}(\text{H}_2\text{O})\text{-O-TRu}^{\text{IV}}(\text{H}_2\text{O})\text{-O-Ru}^{\text{III}}\text{-TB}]^{8+} (\mathbf{1\text{-}tn}^{8+}) + 2\text{MeCN} + 2\text{e}^- \rightarrow [\text{TB-Ru}^{\text{II}}\text{-O-TRu}^{\text{IV}}(\text{MeCN})\text{-O-TRu}^{\text{IV}}(\text{MeCN})\text{-O-Ru}^{\text{II}}\text{-TB}]^{6+} (\mathbf{1\text{-}tn\text{-}N}^{6+}) + 2\text{H}_2\text{O} \quad (4)$$

Addition of acetone to the initial dinuclear complex, **1-dn**$^{4+}$, produces an immediate reduction followed by the oligomerization process that in this case generates trinuclear complex [TB-Ru$^{\text{III}}$-O-TRu$^{\text{IV}}$(H$_2$O)-O-Ru$^{\text{III}}$-TB]$^{6+}$ (**1-tr**$^{6+}$) where the Ru−aqua ligand is maintained as a result of the weak coordination capacity of acetone. In an analogous manner, addition of picolinic acid to a solution of **1-dn**$^{4+}$ generates trinuclear complex **1-tr-P**$^{6+}$, which has a structure similar to that of **1-tr**$^{6+}$ but where the [T-Ru-(H$_2$O)-O] moiety has been substituted by the [P$_2$-Ru-O] group.

Finally, in the presence of bpy but in the absence of organic substrates, the IV,IV oxidation state slowly decays (over about 1 week) to lower oxidation states, giving complexes, such as dimer [TB-Ru$^{\text{III}}$-O-Ru$^{\text{III}}$-TB]$^{4+}$ (**1-dm**$^{4+}$) in 85% yield, whose formation can be monitored by UV−vis spectroscopy (Supporting Information) as a result of the presence of a highly characteristic band at 688 nm (Figure 3).

Taken together, all of the above synthesis results point to the existence of an oligomerization process where the [T-Ru-(H$_2$O)-O] moiety acts as a repeating unit and the [TB-Ru] moiety acts as a stopper to the polymerization process, that is,

$$n[\text{T-Ru}^{\text{IV}}\text{-(O)(OH}_2)_2]^{2+} \rightarrow [\text{T-Ru}^{\text{IV}}\text{-(O)OH}_2]_n^{2n+} + n\text{H}_2\text{O} \quad (5)$$

$$2[\text{TB-Ru}^{\text{III}}\text{-OH}_2]^{3+} + [\text{T-Ru}^{\text{IV}}\text{-(O)OH}_2]_n^{2n+} \rightarrow \{\text{TB-Ru-[O-TRu(H}_2\text{O)]}_n\text{-O-Ru-TB}\}^{(2n+4)+} + 2\text{H}^+ + \text{H}_2\text{O} \quad (6)$$

Depending on time and solubility, oligomers with a different number of repeating units are obtained.

3.2. Ru-O-Ru Structure and Electronic Properties. The crystal structure of all of the Ru−O-bridged complexes discussed in the present Article are displayed in Figure 1. In all cases, the metal center exhibits a distorted octahedral coordination; the most interesting feature of these complexes is their Ru−O−Ru bond distances and angles (summarized in Table 1, together with those of related oxo-bridged Ru complexes previously reported in the literature).

The Ru-O-Ru bonding parameters depend on the oxidation state as well as on the degree of electronic coupling between the metal centers through the oxygen bridging atom. A qualitative molecular orbital diagram for the π system of Ru-O-Ru-type complexes[31,32] is shown in Figure 2; this sheds some light on the orbitals involved in this type of bonding for the Ru-O-Ru moiety

Herein, the Ru−O bond is taken as the z axis; thus, the d_{xz} and d_{yz} orbitals from the metal atoms mix with two π-type p orbitals from the oxo bridging atom, producing three sets of bridge-based orbitals. The first set consists of bonding orbitals (π_1^b, π_2^b) that have large p_O characters. The next set contains two

DOI: 10.1021/ic502603e
Inorg. Chem. 2015, 54, 658−666

Table 1. Comparison of Important Bond Distances (Å) and Angles (deg) for Oxo-Bridge Polynuclear Metal Complexes

complex[a]	$Ru_{(2)}-O_{(2)}$	$Ru_{(2)}-O_{(1)}$	$Ru_{(1)}-O_{(1)}$	$Ru_{(1)}-O-Ru_{(2)}$	ref
Ru^{IV}-$O_{(1)}$-Ru^{IV}					
1-dn^{4+}	1.747(3)[b]	1.832(3)	1.848(3)	175.43(18)	*d*
2-dn^{4+}	1.738(4)[b]	1.830(3)	1.855(3)	171.5(2)	*d*
3-dn^{4+}	1.731(3)[b]	1.833(3)	1.850(3)	172.63(16)	*d*
$\{[(OEP)ClRu^{IV}]_2O\}$[c]		1.793(2)	1.793(2)	180	36
$\{[(OEP)(OH)Ru^{IV}]_2O\}$[c]		1.847(13)	1.847(13)	180	37
$\{[Cl_5Ru^{IV}]_2O\}^{4-}$[c]		1.80	1.80	180	38
Ru^{III}-$O_{(1)}$-Ru^{IV}					
1-dm^{5+}		1.846(2)	1.848(2)	169.90(13)	*d*
$[(bpy)_2(H_2O)Ru^{III}ORu^{IV}(OH)(bpy)_2]^{4+}$		1.847(12)	1.823(12)	170.0(7)	35
$[(bpy)_2(Cl)Ru^{III}ORu^{IV}(Cl)(bpy)_2]^{4+}$		1.845(9)	1.805(9)	170.7(5)	35
$[(TACN)Ru^{III}(O)(CH_3CO_2)_2Ru^{IV}(TACN)]^{3+}$		1.849(5)	1.837(5)	130.1(3)	33
Ru^{III}-$O_{(1)}$-Ru^{III}					
1-dn-N^{4+}[e]		1.864(4)[f]	1.865(4)	169.9(2)	*d*
3-dn-N^{4+}		1.912(5)[f]	1.891(5)	166.1(3)	*d*
1-dm^{4+}		1.8810(12)	1.8819(12)	164.31(7)	*d*
$\{[Ru^{III}(trpy)(C_2O_4)]_2(\mu\text{-}O)\}$		1.846(8)	1.841(8)	148.5(4)	51
$\{[Ru^{III}(TACN)(acac)]_2(\mu\text{-}O)\}^{2+}$		1.913(1)	1.913(1)	180.0(1)	47
$\{[Ru^{III}(bpy)_2(NH_3)]_2(\mu\text{-}O)\}^{4+}$		1.894(2)	1.894(2)	158.2(4)	52
$\{[Ru^{III}(bpy)_2(H_2O)]_2(\mu\text{-}O)\}^{4+}$		1.869(1)	1.869(1)	165.4(3)	53
$\{[Ru^{III}(bpy)_2(NO_2)]_2(\mu\text{-}O)\}^{2+}$		1.876(6)	1.890(7)	157.2(3)	54
$\{[Ru^{III}(TACN)]_2(\mu\text{-}O)(\mu\text{-}CH_3CO_2)_2\}^{2+}$		1.884(2)	1.884(2)	119.7(2)	33
$\{[Ru^{III}(tpm)]_2(\mu\text{-}O)(\mu\text{-}O_2P(O)(OH))_2\}$		1.868(2)	1.868(2)	124.7(4)	32
M^{III}-$O_{(1)}$-Ru^{IV}-O-M^{III}[g,h]					
1-tr-P^{4+}[l]		1.805(5), 1.799(5)[i]	1.872(5), 1.875(5)[j]	173.5(3), 176.6(3)[k]	*d*
1-tr^{6+}		1.821(3)[i]	1.881(3)[j]	166.0(2)[k]	*d*
$\{[(NH_3)_5Ru^{III}(\mu\text{-}O)]_2Ru^{IV}(en)_2\}^{6+}$		1.850(4)[i]	1.891(4)[j]	177.2(4)[k]	55
$\{[(BuNH_2)((DPG)BF_2)_2Fe^{III}(\mu\text{-}O)]_2Ru^{IV}(TPP')\}$[l]		1.796(8), 1.801(8)[i]	1.786(8), 1.788(8)[j]	174.8(5), 175.1(5)[k]	41
$\{[(Salmah)Fe^{III}(\mu\text{-}O)]_2Ru^{IV}(TPP)\}$		1.866(6)[i]	1.848(6)[j]	155.2(5)[k]	56
$Ru^{II}_{(1)}$-$O_{(1)}$-$Ru^{IV}_{(2)}$-$O_{(2)}$-Ru^{IV}-O-Ru^{II}[g]					
1-tn-N^{6+}	1.8496(3)	1.839(2)	1.883(2)	169.67(15)	*d*
2-tn-Ac^{6+}	1.8364(3)	1.823(2)	1.865(3)	169.44(16)	*d*
3-tn-N^{6+}	1.8378(8)	1.829(6)	1.892(6)	168.10(4)	*d*

[a]OEP = octaethylporphinate, TACN = 1,4,7-trimethyl-1,4,7-triazacyclononane, acac = pentane-2,4-dionate, en = ethylenediamine, $BuNH_2$ = *n*-butylamine, $(DPG)BF_2$ = (difluoroboryl)-diphenylglyoximate, TPP′ = tetrakis(4-methoxyphenylporphyrinate), Salmah = *N*,*N*′-(4-methyl-4-azaheptane-1,7-diyl)bis(salicylaldiminaate), TPP = 5,10,15,20-tetraphenylpophyrinate. [b]$Ru_{(2)}$ corresponds to Ru bound to the oxo terminal ligand which is labeled as $O_{(2)}$. [c]High-symmetry complexes where $Ru_{(1)}-O_{bridge} = Ru_{(2)}-O_{bridge}$. [d]This Article. [e]The bipyridine and acetonitrile ligands are disordered and interchange their positions with a ratio of 86:14, which means that $Ru_{(1)}$ and $Ru_{(2)}$ also interchange positions. [f]$Ru_{(2)}$ corresponds to Ru bound to two CH_3CN ligands. [g]Usually centrosymmetric complexes. [h]M^{III} = Ru^{III} in **1-tr-P**$^{4+}$ and **1-tr**$^{6+}$, and M^{III} = Fe^{III} in the remaining complexes. [i]$Ru_{(2)}$ corresponds to the central Ru^{IV} atom. [j]$Ru_{(1)}$ corresponds to the outer M^{III} atoms. [k]$Ru^{IV}-O-M^{III}$ angle. [l]The complex is noncentrosymmetric; a couple of distances or angles are shown in each field.

nonbonding or slightly antibonding orbitals (π_1^{nb}, π_2^{nb}) that have large $d\pi_{Ru}$ characters. The third set comprises two antibonding orbitals (π_1^*, π_2^*) which have also a large $d\pi_{Ru}$ character. For complexes with a linear geometry, that is, with a Ru−O−Ru angle of 180°, π_1^* and π_2^* are degenerate. However, when the Ru−O−Ru angles are smaller than 180°, the degeneracy is lost, and their energy difference is a function of the Ru−O−Ru angle.

Dinuclear oxo bridge d^5 Ru^{III} complexes with large energy gap between π_1^* and π_2^* have $(\pi_1^b)^2$ $(\pi_2^b)^2$ $(\pi_1^{nb})^2$ $(\pi_2^{nb})^2$ $(\pi_1^*)^2$ electronic configuration and thus are diamagnetic. This is the case for $\{[Ru^{III}(TACN)]_2(\mu\text{-}O)(\mu\text{-}CH_3CO_2)_2\}^{2+}$[33] and $\{[Ru^{III}(tpm)]_2(\mu\text{-}O)(\mu\text{-}O_2P(O)(OH))_2\}$,[32] which have Ru−O−Ru angles of 120° and 125°, respectively. In contrast, dinuclear oxo-bridged d^5 Ru^{III} complexes with Ru−O−Ru angles close to 180° display a paramagnetic behavior caused by either the degeneracy of π_1^* and π_2^* or their closeness in energy; thus, both will be populated at room temperature.

In the case of **1-dm**$^{4+}$, the Ru−O−Ru angle is 164°; thus, it has paramagnetic behavior at room temperature that is manifested by the broad range of the chemical shift (−30 to +30 ppm) where the resonances are observed in the ^1H NMR spectrum (Supporting Information). A similar shift has been observed for related Ru^{III}-O-Ru^{III} complexes.[34] The number of signals agrees with two [Ru(trpy)(bpy)] halves manifesting a symmetric configuration in solution.

For the one-electron-oxidized complex, **1-dm**$^{5+}$, the Ru−O distance is shortened by approximately 0.035 Å, which is in agreement with a higher bond order for Ru−O because of the removal of an electron from the antibonding orbital π_2^* as compared to **1-dm**$^{4+}$. In addition, the two Ru−O bonds in **1-dm**$^{5+}$ are almost identical, suggesting a high degree of electronic

DOI: 10.1021/ic502603e
Inorg. Chem. 2015, 54, 658−666

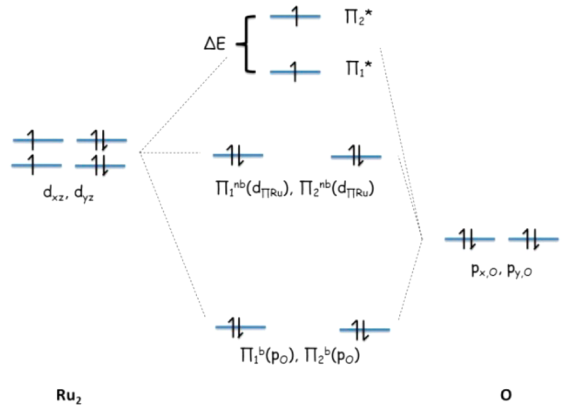

Figure 2. Qualitative molecular orbital diagram for the π system of Ru-O-Ru complexes. ΔE depends on the angle of the moiety: the smaller the angle, the larger the energetic separation. The electronic configuration illustrates the case of a d^5–d^5 Ru^{III}-O-Ru^{III} complex.

coupling between the two Ru metal centers through the oxo bridge.

The dinuclear complexes **1**-, **2**-, and **3-dn**$^{4+}$ have two radically different sites; one is a [TB-Ru^{IV}] moiety and the other a [$TRu^{IV}(O)(H_2O)$] group that generate non-symmetric Ru–O–Ru bonds, as can be observed in Table 1. The same effect has been also found in the III,IV form of the blue dimer.[35] This is in sharp contrast with previously reported[36−38] symmetric complexes where the Ru^{IV}–O–Ru^{IV} bonds are practically identical. Finally in the crystal structure of **3-dn**4+ we find the shortest Ru–O terminal bond ever reported.[39]

This is in sharp contrast with previously reported[36−38] symmetric complexes where the Ru^{IV}–O–Ru^{IV} bonds are practically identical (Table 1). Finally, in the crystal structure of **3-dn**$^{4+}$, we find the shortest Ru–O terminal bond ever reported.[39]

The Ru^{IV}–O–Ru^{IV} angles are slightly bent with respect to the ideal 180° found in previously reported complexes, caused by the steric constraint from the proximity of the bpy ligand to the aquo group. In this way, the less sterically demanding bpy in **1-dn**$^{4+}$ generates a Ru–O–Ru angle of 175.5°, whereas with the more sterically demanding fluoro bpys in **2-dn**$^{4+}$ and **3-dn**$^{4+}$, the angles are 171.5 and 172.6°, respectively.

A related structural motif is shared in complexes **1-dn-N**$^{4+}$ and **3-dn-N**$^{4+}$ (Figure 1, Supporting Information, and Table 1), where the aquo group has been replaced by MeCN and the Ru metal centers are at oxidation state III. As a consequence of this, the Ru–O bond distances are slightly elongated (Table 1).[35]

Two trinuclear complexes with a Ru^{III}-O-Ru^{IV}-O-Ru^{III} backbone have been obtained, **1-tr**$^{6+}$ and **1-tr-P**$^{4+}$ (Figure 1); their structures are reminiscent of ruthenium red,[40] $\{[(NH_3)_5Ru^{III}(\mu\text{-}O)]_2[\mu\text{-}Ru^{IV}(NH_3)_4]\}^{6+}$. There are only a few crystallographically characterized trinuclear Ru–O-bridged complexes, including some heterotrinuclear ones[41] where the Ru is situated at the central position in oxidation state IV (Table 1). In **1-tr**$^{6+}$, the central Ru atom adopts a *trans*-dioxo arrangement and bears an aquo ligand. The Ru^{IV}–O and Ru^{III}–O distances are significantly different, suggesting a weak coupling among metallic atoms. (Table 1) The trans–dioxo nature of the central Ru together with the presence of the aqua ligand attached to the same metal center converts it into a potentially powerful WOC.[19]

The main structural parameters for **1-tr-P**$^{4+}$ are also collected in Table 1. As in the previous case, the Ru^{IV}–O distance is considerably shorter than that of Ru^{III}–O (Δd = 0.078 Å), suggesting another weak electronic coupling. It is worth mentioning that the Ru^{IV}–$O_{carboxylate}$ bond (2.034 Å) is shorter than that reported[42−44] for mononuclear picolinate Ru^{II} complexes (2.085–2.102 Å) and similar to that described[45] in a Ru^{IV} pyridinecarboxylate compound (2.068(3) Å), supporting the oxidation state assignment.

Tetranuclear complexes **1-tn-N**$^{6+}$ and **3-tn-N**$^{6+}$ with the $Ru^{II}_{(1)}$-$O_{(1)}$-$Ru^{IV}_{(2)}$-$O_{(2)}$-$Ru^{IV}_{(2')}$-$O_{(1')}$-$Ru^{II}_{(1')}$ backbone have also been obtained. Their ORTEP plots are presented in Figure 1 and the Supporting Information, and selected bond distances and angles from these complexes are displayed in Table 1. These complexes contain an inversion center, *i*, situated at the central $O_{(2)}$ atom. For complex **1-tn-N**$^{6+}$, the $Ru_{(1)}$–O distance is 1.88 Å, which is significantly longer than the $Ru_{(2)}$–O distances (1.85 and 1.84 Å). These Ru–O bonding distances suggest a [$(Ru^{II}$-O-$Ru^{IV})_2$-(μ-O)] assignment rather than a [$(Ru^{III}$-O-$Ru^{III})_2$-(μ-O)] one, which would also be in agreement with the overall charge of the cationic component of the molecule. A similar analysis can be carried out for **3-tn-N**$^{6+}$. However, the two-electron-oxidized complex, **3-tn-Ac**$^{6+}$, wherein the MeCN ligands have been substituted by acetate acting as a monodentate ligand, has similar $Ru_{(2)}$–O distances but slightly shorter $Ru_{(1)}$–O distances, supporting a [$(Ru^{III}$-O-$Ru^{IV})_2$-(μ-O)] assignment. This, in turn, also supports the [$(Ru^{II}$-O-$Ru^{IV})_2$-(μ-O)] assignment for **1-tn**$^{6+}$ and **3-tn**$^{6+}$ rather than the intermediate oxidation state options, such as [$(Ru^{II.5}$-O-$Ru^{III.5})_2$-(μ-O)]; further spectroscopic analysis is needed for complete characterization of the oxidation state.

3.3. Chemistry Related to 1-dm^{4+}**.** As mentioned in the synthesis section (section 3.1), **1-dm**$^{4+}$ can be obtained in high yield by adding 100 equiv of Ce^{IV} to a 0.1 M aqueous solution of triflic acid containing 1 equiv of **1**$^{2+}$. As reported earlier,[19] this generates a system containing two parallel catalytic systems that are based on the oxidation of **1**$^{2+}$ and the formation of **1-dn**$^{4+}$ arising from bpy loss from the former, as indicated in eq 1. Once Ce^{IV} is depleted, the two catalytic cycles stop generating species at high oxidation states, such as [trpy-bpy-Ru^{IV}=O]$^{2+}$ and **1-dn**$^{4+}$. These species are not stable in acidic solution and decay slowly to lower-oxidation-state species in the presence of free bpy. Over a period of 1 week, this mix decays mainly to **1-dm**$^{4+}$ (85% yield judging from UV–vis).

Complex **1-dm**$^{4+}$ has been characterized in solution by UV–vis and NMR spectroscopy and in the solid state by X-ray diffraction analysis, as shown in section 3.2. Additionally, the complex has been characterized electrochemically by means of CV and DPV, and its reactivity was tested upon addition of a large excess of Ce^{IV}.

The UV–vis spectrum of **1-dm**$^{4+}$ in a 0.1 M solution of triflic acid is displayed in Figure 3. The most interesting feature of this spectrum is the band at 688 nm that is typical of Ru^{III}-O-Ru^{III} type of complexes[46,47] and is associated with the overlapping of MLCT and bridge-based transitions.[48,49] Interestingly, the oxidation of mononuclear complexes **1**$^{2+}$ and **2**$^{2+}$ with only 2 or 3 equiv of Ce^{IV} also produces this band, manifesting the tendency toward oxo bridge formation in mononuclear systems. ^{1}H NMR at room temperature for paramagnetic complex **1-dm**$^{4+}$ was also registered in 0.1 M CF_3SO_3D in D_2O. The spectrum shows resonances in a very wide range, which is caused by the paramagnetic shift exerted by the Ru^{III} d^5 ions. A DOSY experiment was also carried out

DOI: 10.1021/ic502603e
Inorg. Chem. 2015, 54, 658–666

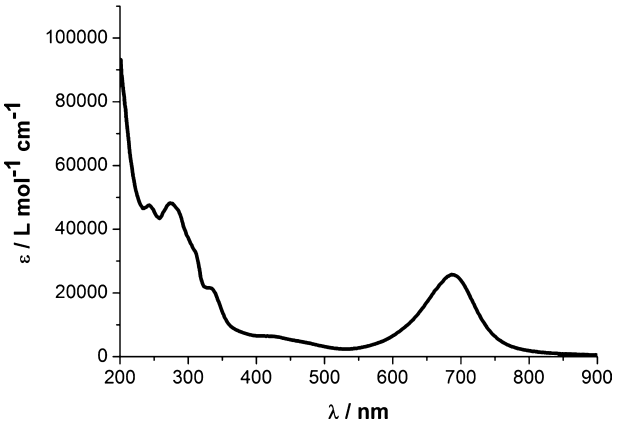

Figure 3. UV−vis spectrum of **1-dm**$^{4+}$ in 0.1 M HOTf.

that nicely reflects that the hydrodynamic radius according to the Stokes−Einstein equation is 1.9 times larger than that of $[Ru(trpy)(bpy)(MeCN)]^{2+}$, used as a mononuclear standard.

The CV of **1-dm**$^{4+}$ in 0.1 M triflic acid is depicted in Figure 4. The initial anodic scan from the open-circuit potential up to

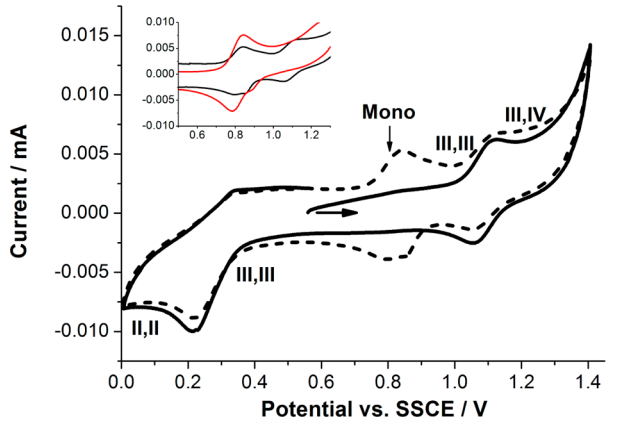

Figure 4. CV of **1-dm**$^{4+}$ in 0.1 M HOTf: (solid line) 1st cycle and (dashed line) 2nd cycle. The inset shows a comparison of the second cycle (black) and a CV from a solution of $\mathbf{1}^{2+}$ (red) in the same solvent. Polished glassy carbon was used as the working electrode, a Pt wire was used as the counter electrode, and SSCE was used as the reference electrode. Scan rate = 100 mV s^{-1}.

1.40 V shows a reversible wave at $E_{1/2}$ = 1.08 V (ΔE = 55 mV). This electrochemical process is attributed to the one-electron-oxidation in eq 1, as previously reported[46,47] for related complexes.

$$Ru^{III}\text{-}O\text{-}Ru^{III} - 1e^- \rightarrow Ru^{III}\text{-}O\text{-}Ru^{IV} \quad E_{1/2} = 1.08\ V \tag{7}$$

After a subsequent cathodic scan until 0 V, a chemically irreversible wave appears at $E_{p,c}$ = 0.22 V, which is consistent with the 2e$^-$/1H$^+$ transfer indicated in eq 8, as reported in the literature for related complexes, followed by Ru−O bond breaking and formation of mononuclear complex $\mathbf{1}^{2+}$.

$$Ru^{III}\text{-}O\text{-}Ru^{III} + 2e^- + H^+ \rightarrow Ru^{II}\text{-}(OH)\text{-}Ru^{II} \quad E_{p,c} = 0.22\ V \tag{8}$$

$$Ru^{II}\text{-}(OH)\text{-}Ru^{II} + H_2O + H^+ \rightarrow 2Ru^{II}\text{-}OH_2 \tag{9}$$

This is clearly seen in the second CV cycle where a new chemically reversible wave and a new electrochemically quasireversible wave, which are both associated with $\mathbf{1}^{2+}$, appear at E^0 = 0.82 V and E^0 = 0.98 V, respectively.

Addition of 100 equiv of Ce^{IV} to **1-dm**$^{4+}$ generates oxygen with a TN of 7.6 and a TOF$_i$ of 6.19 h^{-1}, which can be extracted from the oxygen-generation profile as a function of time (Supporting Information). This was a surprising result because **1-dm**$^{4+}$ was not expected to be an active WOC, given the absence of an aqua group bonded to the Ru metal. To decipher what the active species were, we followed the reaction by RR spectroscopy.

Figure 5 shows the RR spectrum of **1-dm**$^{4+}$ in 0.1 M triflic acid before the addition of Ce^{IV} (black line). After addition of

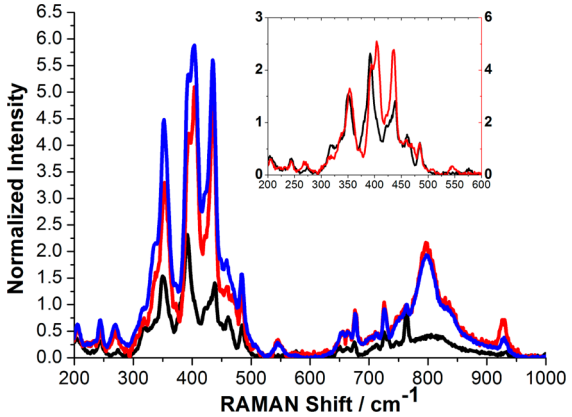

Figure 5. Resonance Raman spectra: (red) 30 s and (blue) 2.73 h after the addition of 100 equiv of CAN to a 1 mM solution of **1-dm**$^{4+}$ in 0.1 M HOTf at 25 °C. The spectrum before the reaction is also included (black). Inset shows an enlargement of the 200−600 cm^{-1} region.

Ce^{IV}, two spectra were recorded: one after 30 s (red line) and the second one after 2.73 h (blue line). First, a vibration with high intensity at 392 cm^{-1}, observed in the spectrum of **1-dm**$^{4+}$ before oxidant addition and caused by the ν_S Ru−O−Ru mode,[35,49,50] shifts to 404 cm^{-1}. This blueshift is in agreement with a higher bond order of the Ru−O−Ru moiety; thus, it can be associated with the one-electron oxidation of the initial dimer to form **1-dm**$^{5+}$. Incidentally, addition of a large amount of ClO_4^- to this solution generates nice brown crystals of **1-dm**$^{5+}$ that confirm this assignment. Second, surprisingly, the spectra at 30 s and 2.73 h each present a vibration at 801 cm^{-1} that is the typical signature of **1-dn**$^{4+}$, as we have reported earlier.[19] This clearly suggests that upon addition of Ce^{IV} the **1-dm**$^{4+}$ dimer partially reorganizes to form a small amount of **1-dn**$^{4+}$; this, in turn, is responsible for the observed catalytic oxygen generation, as we have demonstrated earlier. No RuO_2 was detected in our experiments, which is in agreement with the oxidative robustness of the ligands used and the stability of the Ru−oxo-bridged moiety. The formation of RuO_2 as a black solid is very obvious when using Ru complexes with ligands that are easy to oxidize, which typically contain benzylic-, pyridyl-benzyllic-, or amine-type groups.[57,58] We also have a nice correlation of dimer formation and oxygen generation[19] that is again in agreement with the absence of RuO_2 in our systems.

4. CONCLUSIONS

Mononuclear $[TBRu^{II}\text{-}OH_2]$ complexes behave as WOCs in the presence of a large excess of Ce^{IV}. In parallel, these

DOI: 10.1021/ic502603e
Inorg. Chem. 2015, 54, 658−666

mononuclear complexes also suffer from ligand loss and the formation of dinuclear oxo-bridged complexes that are also active WOCs. As expected, their high oxidation states are also highly active agents for the oxidation of organic substrates, producing a series of polynuclear complexes at reduced oxidation states and illustrating the existence of an oligomerization process.

We have isolated dinuclear, trinuclear, and tetranuclear oxo-bridged complexes that have been structurally characterized by single-crystal X-ray diffraction analysis. The structural properties of these complexes have been correlated to their electronic structure.

Finally, the structural, electrochemical, and reactivity properties of oxo-bridged dimer **1-dm**$^{4+}$ have been thoroughly studied. In particular, RR spectroscopy clearly shows that the observed catalytic oxidation of water to dioxygen is due to a reorganization of **1-dm**$^{4+}$ into **1-dn**$^{4+}$ after the addition of Ce^{IV}.

■ ASSOCIATED CONTENT

Supporting Information

Additional spectroscopic, electrochemical, and reactivity experiments; crystallographic information; and CIF files (CCDC nos. 1016623−1016632). This material is available free of charge via the Internet at http://pubs.acs.org.

■ AUTHOR INFORMATION

Corresponding Author

*E-mail: allobet@iciq.cat.

Notes

The authors declare no competing financial interest.

■ ACKNOWLEDGMENTS

Support from MINECO (CTQ-2013-49075-R, SEV-2013-0319 and PRI-PIBIN-2011-1278) is gratefully acknowledged. S.M. thanks MINECO for a Torres Quevedo contract, and I.L. is grateful for an FPU grant.

■ REFERENCES

(1) Bertini, I.; Lalli, D.; Mangani, S.; Pozzi, C.; Rosa, C.; Theil, E. C.; Turano, P. *J. Am. Chem. Soc.* **2012**, *134*, 6169.

(2) Tshuva, E. Y.; Lippard, S. J. *Chem. Rev. (Washington, DC, U.S.)* **2004**, *104*, 987.

(3) Vincent, J. B.; Olivier-Lilley, G. L.; Averill, B. A. *Chem. Rev. (Washington, DC, U.S.)* **1990**, *90*, 1447.

(4) Sens, C.; Romero, I.; Rodríguez, M.; Llobet, A.; Parella, T.; Benet-Buchholz, J. *J. Am. Chem. Soc.* **2004**, *126*, 7798.

(5) Zong, R.; Thummel, R. P. *J. Am. Chem. Soc.* **2005**, *127*, 12802.

(6) Deng, Z.; Tseng, H.-W.; Zong, R.; Wang, D.; Thummel, R. *Inorg. Chem.* **2008**, *47*, 1835.

(7) Xu, Y.; Åkermark, T.; Gyollai, V.; Zou, D.; Eriksson, L.; Duan, L.; Zhang, R.; Åkermark, B.; Sun, L. *Inorg. Chem.* **2009**, *48*, 2717.

(8) Karlsson, E. A.; Lee, B.-L.; Åkermark, T.; Johnston, E. V.; Kärkäs, M. D.; Sun, J.; Hansson, Ö.; Bäckvall, J.-E.; Åkermark, B. *Angew. Chem., Int. Ed.* **2011**, *50*, 11715.

(9) Sartorel, A.; Miro, P.; Salvadori, E.; Romain, S.; Carraro, M.; Scorrano, G.; Valentin, M. D.; Llobet, A.; Bo, C.; Bonchio, M. *J. Am. Chem. Soc.* **2009**, *131*, 16051.

(10) Geletii, Y. V.; Botar, B.; Kögerler, P.; Hillesheim, D. A.; Musaev, D. G.; Hill, C. L. *Angew. Chem., Int. Ed.* **2008**, *47*, 3896.

(11) Yin, Q.; Tan, J. M.; Besson, C.; Geletii, Y. V.; Musaev, D. G.; Kuznetsov, A. E.; Luo, Z.; Hardcastle, K. I.; Hill, C. L. *Science* **2010**, *328*, 342.

(12) Lv, H.; Geletii, Y. V.; Zhao, C.; Vickers, J. W.; Zhu, G.; Luo, Z.; Song, J.; Lian, T.; Musaev, D. G.; Hill, C. L. *Chem. Soc. Rev.* **2012**, *41*, 7572.

(13) Concepcion, J. J.; Jurss, J. W.; Templeton, J. L.; Meyer, T. J. *J. Am. Chem. Soc.* **2008**, *130*, 16462.

(14) Tseng, H.-W.; Zong, R.; Muckerman, J. T.; Thummel, R. *Inorg. Chem.* **2008**, *47*, 11763.

(15) Concepcion, J. J.; Tsai, M.-K.; Muckerman, J. T.; Meyer, T. J. *J. Am. Chem. Soc.* **2010**, *132*, 1545.

(16) Wasylenko, D. J.; Ganesamoorthy, C.; Henderson, M. A.; Koivisto, B. D.; Osthoff, H. D.; Berlinguette, C. P. *J. Am. Chem. Soc.* **2010**, *132*, 16094.

(17) Polyansky, D. E.; Muckerman, J. T.; Rochford, J.; Zong, R.; Thummel, R. P.; Fujita, E. *J. Am. Chem. Soc.* **2011**, *133*, 14649.

(18) Wasylenko, D. J.; Ganesamoorthy, C.; Koivisto, B. D.; Henderson, M. A.; Berlinguette, C. P. *Inorg. Chem.* **2010**, *49*, 2202.

(19) López, I.; Ertem, M. Z.; Maji, S.; Benet-Buchholz, J.; Keidel, A.; Kuhlmann, U.; Hildebrandt, P.; Cramer, C. J.; Batista, V. S.; Llobet, A. *Angew. Chem., Int. Ed.* **2014**, *53*, 205.

(20) *Activation of Small Molecules*; Tolman, W. B., Ed.; WILEY-VCH: Weinheim, Germany, 2006.

(21) Suzuki, M. *Acc. Chem. Res.* **2007**, *40*, 609.

(22) Cramer, C. J.; Tolman, W. B. *Acc. Chem. Res.* **2007**, *40*, 601.

(23) Takeuchi, K. J.; Thompson, M. S.; Pipes, D. W.; Meyer, T. J. *Inorg. Chem.* **1984**, *23*, 1845.

(24) Maji, S.; López, I.; Bozoglian, F.; Benet-Buchholz, J.; Llobet, A. *Inorg. Chem.* **2013**, *52*, 3591.

(25) *APEX2* , version 2009.1−0.2; Bruker AXS, Inc.: Madison, WI, 2009.

(26) *SAINT*, version 7.60A; Bruker AXS, Inc.: Madison, WI, 2007.

(27) Sheldrick, G. *Acta Crystallogr., Sect. A* **2008**, *64*, 112.

(28) Spek, A. *J. Appl. Crystallogr.* **2003**, *36*, 7.

(29) Zanella, A. W.; Ford, P. C. *Inorg. Chem.* **1975**, *14*, 42.

(30) Mola, J.; Pujol, D.; Rodríguez, M.; Romero, I.; Sala, X.; Katz, N.; Parella, T.; Benet-Buchholz, J.; Fontrodona, X.; Llobet, A. *Aust. J. Chem.* **2009**, *62*, 1675.

(31) Weaver, T. R.; Meyer, T. J.; Adeyemi, S. A.; Brown, G. M.; Eckberg, R. P.; Hatfield, W. E.; Johnson, E. C.; Murray, R. W.; Untereker, D. *J. Am. Chem. Soc.* **1975**, *97*, 3039.

(32) Llobet, A.; Curry, M. E.; Evans, H. T.; Meyer, T. J. *Inorg. Chem.* **1989**, *28*, 3131.

(33) Neubold, P.; Wieghardt, K.; Nuber, B.; Weiss, J. *Inorg. Chem.* **1989**, *28*, 459.

(34) Dobson, J. C.; Sullivan, B. P.; Doppelt, P.; Meyer, T. J. *Inorg. Chem.* **1988**, *27*, 3863.

(35) Schoonover, J. R.; Ni, J.; Roecker, L.; White, P. S.; Meyer, T. J. *Inorg. Chem.* **1996**, *35*, 5885.

(36) Masuda, H.; Taga, T.; Osaki, K.; Sugimoto, H.; Mori, M.; Ogoshi, H. *Bull. Chem. Soc. Jpn.* **1982**, *55*, 3887.

(37) Masuda, H.; Taga, T.; Osaki, K.; Sugimoto, H.; Mori, M.; Ogoshi, H. *J. Am. Chem. Soc.* **1981**, *103*, 2199.

(38) Deloume, J. P.; Faure, R.; Thomas-David, G. *Acta Crystallogr., Sect. B* **1979**, *35*, 558.

(39) Che, C. M.; Tang, W. T.; Wong, W. T.; Lai, T. F. *J. Am. Chem. Soc.* **1989**, *111*, 9048.

(40) Fletcher, J. M.; Greenfield, B. F.; Hardy, C. J.; Scargill, D.; Woodhead, J. L. *J. Chem. Soc.* **1961**, 2000.

(41) Vernik, I.; Stynes, D. V. *Inorg. Chem.* **1998**, *37*, 10.

(42) Barral, M. C.; Jimenez-Aparicio, R.; Royer, E. C.; Saucedo, M. J.; Urbanos, F. A.; Gutierrez-Puebla, E.; Ruiz-valero, C. *J. Chem. Soc., Dalton Trans.* **1991**, 1609.

(43) Biswas, M. K.; Patra, S. C.; Maity, A. N.; Ke, S.-C.; Weyhermuller, T.; Ghosh, P. *Chem. Commun. (Cambridge, U.K.)* **2013**, *49*, 4522.

(44) Carter, L.; Davies, D. L.; Fawcett, J.; Russell, D. R. *Polyhedron* **1993**, *12*, 1599.

(45) Sahli, Z.; Derrien, N.; Pascal, S.; Demerseman, B.; Roisnel, T.; Barriere, F.; Achard, M.; Bruneau, C. *Dalton Trans.* **2011**, *40*, 5625.

(46) Llobet, A.; Doppelt, P.; Meyer, T. J. *Inorg. Chem.* **1988**, *27*, 514.

(47) Schneider, R.; Weyhermueller, T.; Wieghardt, K.; Nuber, B. *Inorg. Chem.* **1993**, *32*, 4925.

DOI: 10.1021/ic502603e
Inorg. Chem. 2015, 54, 658−666

(48) Liu, F.; Concepcion, J. J.; Jurss, J. W.; Cardolaccia, T.; Templeton, J. L.; Meyer, T. J. *Inorg. Chem.* **2008**, *47*, 1727.
(49) Jurss, J. W.; Concepcion, J. J.; Butler, J. M.; Omberg, K. M.; Baraldo, L. M.; Thompson, D. G.; Lebeau, E. L.; Hornstein, B.; Schoonover, J. R.; Jude, H.; Thompson, J. D.; Dattelbaum, D. M.; Rocha, R. C.; Templeton, J. L.; Meyer, T. J. *Inorg. Chem.* **2012**, *51*, 1345.
(50) Sanders-Loehr, J.; Wheeler, W. D.; Shiemke, A. K.; Averill, B. A.; Loehr, T. M. *J. Am. Chem. Soc.* **1989**, *111*, 8084.
(51) Lebeau, E. L.; Adeyemi, S. A.; Meyer, T. J. *Inorg. Chem.* **1998**, *37*, 6476.
(52) Ishitani, O.; White, P. S.; Meyer, T. J. *Inorg. Chem.* **1996**, *35*, 2167.
(53) Gilbert, J. A.; Eggleston, D. S.; Murphy, W. R.; Geselowitz, D. A.; Gersten, S. W.; Hodgson, D. J.; Meyer, T. J. *J. Am. Chem. Soc.* **1985**, *107*, 3855.
(54) Phelps, D. W.; Kahn, E. M.; Hodgson, D. J. *Inorg. Chem.* **1975**, *14*, 2486.
(55) Earley, J. E.; Smith, P. M.; Fealey, T.; Silverton, J. V. *Inorg. Chem.* **1971**, *10*, 1943.
(56) Schulz, L. D.; Fallon, G. D.; Moubaraki, B.; Murray, K. S.; West, B. O. *J. Chem. Soc., Chem. Commun.* **1992**, 971.
(57) Francas, L.; Sala, X.; Escudero-Adan, E.; Benet-Buchholz, J.; Escriche, L.; Llobet, A. *Inorg. Chem.* **2011**, *50*, 2771−2781.
(58) Sala, X.; Maji, S.; Bofill, R.; García-Antón, J.; Escriche, L.; Llobet, A. *Acc. Chem. Res.* **2014**, *47*, 504−516.

DOI: 10.1021/ic502603e
Inorg. Chem. 2015, 54, 658−666